Electro- and Photodriven Phase Change Composites Based on Wax-Infiltrated Carbon Nanotube Sponges

Liangjie Chen,[†] Ruqiang Zou,[†,*] Wei Xia,[†] Zhenpu Liu,[†] Yuanyuan Shang,[†] Jinlong Zhu,[‡] Yingxia Wang,[§] Jianhua Lin,[§] Dingguo Xia,[†] and Anyuan Cao[†,*]

[†]Department of Materials Science and Engineering, College of Engineering, Peking University, Beijing 100871, People's Republic of China, [‡]Lujan Neutron Scattering Center, Los Alamos National Laboratory, Los Alamos, New Mexico 87545, United States, and [§]College of Chemistry and Molecular Engineering, Peking University, Beijing 100871, People's Republic of China

ABSTRACT Organic phase change materials are usually insulating in nature, and they are unlikely to directly trigger latent heat storage through an electrical way. Here we report a multifunctional phase change composite in which the energy storage can be driven by small voltages (*e.g.*, 1.5 V) or light illumination with high electro-to-heat or photo-to-thermal storage efficiencies (40% to 60%). The composite is composed of paraffin wax infiltrated into a porous, deformable carbon nanotube sponge; the latter not only acts as a flexible encapsulation scaffold for wax but also maintains a highly conductive network during the phase change process (for both solid and liquid states). Uniform interpenetration between the nanotube network and paraffin wax with high affinity results in enhanced phase change enthalpy and thermal conductivity compared to pure paraffin wax. Our phase change composite can store energy in practical ways such as by sunlight absorption or under voltages applied by conventional lithium-ion batteries.

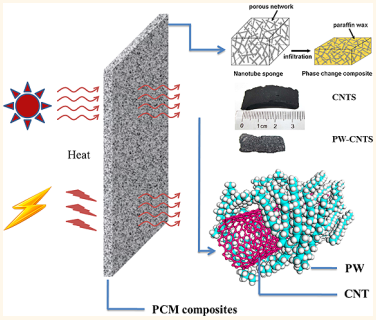

KEYWORDS: phase change material · carbon nanotube sponge · nanocomposite · thermal energy storage

Latent heat storage of phase change materials (PCMs) is a promising way to utilize thermal energy coming from the surrounding environment, solar irradiation, and waste heat produced by vehicles and electronic products.[1−4] Organic solid−liquid PCMs have been studied extensively owing to their moderate phase change enthalpies, wide melting temperatures for convenient use, chemical stability, and abundance in natural resources.[5−7] However, practical applications of organic PCMs have been hindered by a number of challenges including their low thermal conductivity and considerable volume expansion related to phase change that may result in leakage during repeated use.[8−10] Efficient energy storage and conversion by PCMs requires substantial enhancement in thermal conductivity as well as appropriate encapsulation structures without compromising the material enthalpy.

There have been intensive efforts in improving thermal properties and exploring potential encapsulation methods for organic PCMs. The most straightforward way to tailor the thermal properties of a PCM is to introduce nanoscale or microscale fillers to constitute additional thermal transport paths within the organic matrix, and the system thermal conductivities have been enhanced by adding carbon nanotubes (an increase of 40%), graphite, graphene sheets (up to 140%), or carbon fibers with much bigger size (240%).[11−13] In general, mixing excessive conductive fillers into PCMs leads to an obvious decrease of the effective thermal enthalpy in unit mass; for example, the enthalpy of 1-octadecanol decreased by 15.4% after adding 4 wt % graphene sheets.[12] On the other hand, organic PCMs have been encapsulated as microspheres or dispersed into the micropores of polymeric films.[5,14] In those methods, the additional materials used for encapsulation usually have little contribution to heat storage, and the large volume change of PCM contained in the microspheres may cause the outer shells to rupture.

The fabrication and applications of PCM composites dispersed with carbon nanomaterial powders are limited by several factors;

* Address correspondence to rzou@pku.edu, anyuan@pku.edu.cn.

Received for review September 18, 2012 and accepted November 16, 2012.

Published online November 17, 2012
10.1021/nn304310n

© 2012 American Chemical Society

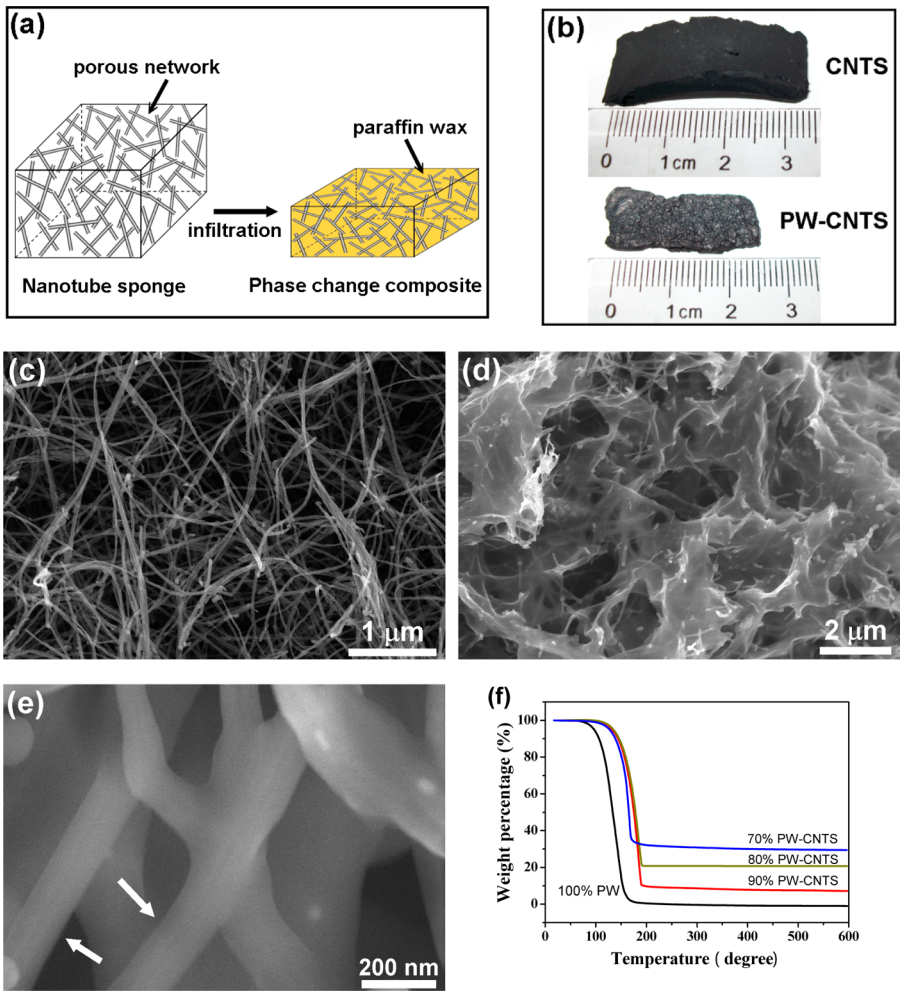

Figure 1. Fabrication and characterization of PW–CNTS composites. (a) Illustration of the fabrication process in which paraffin wax solution was infiltrated to the porous carbon nanotube sponge to make a composite. (b) Photos of an original sponge and the composite after PW infiltration. (c) SEM image of the inner part of the sponge showing a highly porous structure. (d) SEM image of the composite showing the presence of wax membranes in the pores. (e) Enlarged view of individual nanotubes wrapped by wax (see arrows). (f) TGA curves of a pure PW (100%) and three composites with different weight percentages of PW encapsulated in the sponge.

for example, nanomaterials tend to aggregate at higher weight percentages and the composite shape is not fixed (PCM matrix collapses upon melting). Furthermore, the overall structure is still electrically insulating; therefore electroheat conversion is impossible on such PCM composites. Even carbon nanomaterials can form a percolated network through the matrix at increasing loadings, the composite conductivity is too low to be driven by modest voltages, and the network is not stable at elevated temperature when the PCM becomes a fluid. Recently, Zheng *et al*. reported a 2 orders of magnitude change of conductivity in a graphite–hexadecane suspension due to the internal stress generated during the phase change,[15] and this conductivity drops rapidly from the solid to liquid state, hence is not stable. Here, we adopt a carbon nanotube sponge (CNTS) as a porous scaffold to encapsulate paraffin wax (PW) and make an electrically conductive composite with enhanced phase change enthalpy and thermal conductivity. Efficient thermal energy storage in this composite can be realized by means of practical importance such as electroheat conversion or light absorption.

RESULTS AND DISCUSSION

The composite fabrication process simply involves solvent-assisted infiltration of PW into the inner pores of a nanotube sponge. The resulting composite, denoted as PW–CNTS, consists of a three-dimensional nanotube scaffold in which the spacing between the nanotubes is completely or partially filled by PW, as illustrated in Figure 1a. Macroscopic sponges were synthesized by chemical vapor deposition in which multiwalled nanotubes, with diameters of 20 to 30 nm and lengths of tens of μm, were overlapped into an isotropic porous structure by self-assembly, as reported by our group recently.[16,17] The sponges can be compressed to large strains or deformed to arbitrary shapes and then recover original shape without visible plastic deformation. Figure 1b shows a piece of bulk

CNTS in freestanding form (34.5 × 13.9 × 3.9 mm^3) before and after infiltration of PW. Because the porosity of CNTS is more than 99%, it allows infiltration of PW at very high weight percentage (96 wt % in our experiments). To ensure uniform distribution of PW within the pores, the infiltration process is facilitated by dripping a paraffin solution into the sponge with controlled concentration (see Methods for details). Because the CNTS is a bulk material (not powders), solvent-assisted infiltration is a simple and reliable method to make composites. Molten wax (*versus* solution) would be hard to infiltrate directly due to its high viscosity. There might be issues such as local porosity especially at lower wax loadings. During infiltration, wax flows to the inner part of the sponge and is stored within the pores between adjacent nanotubes. After infiltration, the PW–CNTS composite shows significant volume shrinkage to about 26.4 × 11.5 × 1.1 mm^3, which is only 18% of its original state, due to the densification effect induced by solvent evaporation in the drying process (Figure 1b). This property also indicates that the sponge can sustain volume expansion or shrinkage, which is useful for encapsulating phase change materials and accommodating their volume change during melting or freezing. Scanning electron microscopy (SEM) characterization of the original sponge reveals overlapped nanotubes forming a highly porous structure with pore sizes (or average internanotube distances) on the order of a few hundreds of nm to 1 μm (Figure 1c), with a material surface area of >300 m^2/g and a combustion temperature of 570 °C in air (Supporting Information, Figure S1). The empty volumes between nanotubes interconnect with each other throughout the sponge and are accessible by PW through liquid infiltration.

A cross-sectional SEM image of a PW–CNTS composite shows that the nanotubes are wrapped by PW membranes and the internanotube spacing has been filled by PW as well (Figure 1d). Numerous nano- to microscale pores collectively suck PW (enabled by capillarity) and prevent its flowing out during melting or under compression. This is proved by heating the PW–CNTS composite at elevated temperature (60 °C) continuously for a period of two weeks, which remains stable without leakage. We can see that the PW is wetting the nanotubes and forming a good contact by wrapping around the nanotube surface (Figure 1e), and also because the composite is deformable under compression or expansion, the PW and nanotubes could maintain close contact during phase change without forming gaps. This is important for improving the thermal conductivity of PW and also maintaining efficient energy transfer across the PW–nanotube interface. The composite shows a similar morphology after several phase change cycles, indicating that the wax melting and solidification within the sponge is a reversible process, and the composite could maintain the original porous structure (Figure S2). We have made PW–CNTS composites with controlled PW weight percentages from 70% to 90% determined by thermogravimetric analysis (TGA) (Figure 1f). The TGA results show that the combustion temperature of the sponge-encapsulated PW (nearly 200 °C) is higher than the pure PW (about 150 °C), suggesting mutual interactions between the PW and nanotubes.

Phase change behavior was characterized by differential scanning calorimetry (DSC). Figure 2a and Figure S3 summarize the DSC curves of a pure PW (without sponge encapsulation) and six PW–CNTS composites with PW loadings from 76% to 96%. The PW used here has a melting temperature of about 20 °C, and its DSC plot shows an onset point of 20.3 °C with a peak position at 24 °C. In comparison, the onset points of all the composite samples shift to higher temperature and fall in a range of 22.7 to 24.0 °C, and the peak positions increase by 3 degrees to above 27 °C. Considering that the high-density nanotube networks are uniformly embedded among the PW matrix, they could possibly influence the surrounding organic molecules such that the structure change of PW is delayed, resulting in increased phase change temperature of the composite.

Phase change enthalpy can be calculated by the DSC curve based on the enclosed area under the curve during melting (Figure S4). Without sponge encapsulation, pure PW has an absolute enthalpy of 136.0 J/g. For PW–CNTS composites, the apparent enthalpy (including the mass of nanotubes) increases almost linearly with increasing wax loading. At PW loadings of <87 wt %, the apparent enthalpy values are lower than that of pure PW due to a certain weight fraction of carbon nanotubes contained in the composite. In spite of the mixture rule, our results show that above a critical loading of 91 wt %, the composite enthalpy (138.2 J/g) becomes higher than PW (Figure 2b). Both composite enthalpy reduction and enhancement have been observed previously in PCM containing dispersed carbon nanotube fillers.[14,18–20] In particular, an enthalpy increase of 24% in core–shell PCM microspheres was reported recently, although the fabrication of core–shell structures is rather complex and the microspheres need to be further enclosed into a rubber matrix for applications.[14] One can calculate the absolute PW enthalpy by the apparent value divided by the corresponding PW loading, resulting in absolute values of about 148 to 152 J/g, which are about 10% above the pure PW (Figure S5). This 10% increase of PW enthalpy is independent of the PW loading, which is due to the wax–nanotube interaction present in the composites. Measurements on another alkane-based phase change material, eicosane, with a higher original enthalpy (242 J/g), show a *ca.* 6% increase in absolute enthalpy for a 79 wt % eicosane–sponge composite (Figure S6).

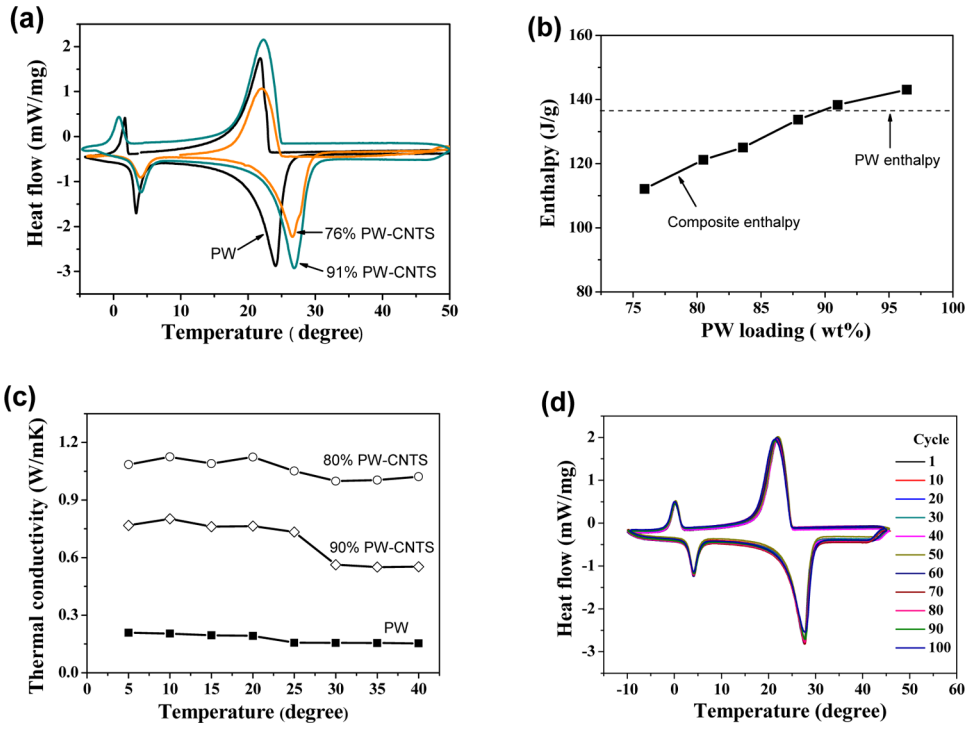

Figure 2. Thermal properties of PW–CNTS composites. (a) DSC curves of unencapsulated PW and two PW–CNTS composites with PW weight percentages of 76% and 91%, respectively. (b) Measured phase change enthalpy of PW–CNTS composites with different PW loadings compared with pure PW (dashed line: 136 J/g). (c) Thermal conductivities of pure PW and two composites with PW weight percentages of 80% and 90%, respectively, recorded across a temperature range of 5 to 40 °C. (d) Collection of DSC curves of a 90.5 wt % PW–CNTS composite tested for 100 cycles, showing very little drift at both high and low temperatures during the heating and cooling processes.

The presence of nanotube networks could have a profound influence on the thermal behavior of PW–CNTS composites, given that individual nanotubes have very high thermal conductivity (>3000 $W \cdot m^{-1} \cdot K^{-1}$).[21] We have measured thermal conductivity by the hot-wire method at temperatures from 5 to 40 °C. The hot wire method is an absolute thermal conductivity technique for measuring gas, liquids, nanofluids, and solids with very low uncertainty.[22] As a control sample, pure PW exhibits a very low conductivity of 0.16 to 0.20 $W \cdot m^{-1} \cdot K^{-1}$. After encapsulation, the composite thermal conductivities reach about 1.2 $W \cdot m^{-1} \cdot K^{-1}$ with a PW loading of 80 wt %, which represent a nearly 6-fold enhancement (Figure 2c). Notably, the thermal conductivity in the liquid state (~1 $W \cdot m^{-1} \cdot K^{-1}$) remains close to that measured in the solid state, while for a graphene–hexadecane suspension, its conductivity drops substantially (by 3 times) during phase change.[15] This is because the nanotube networks are not disturbed by PW melting and maintain a stable structure. Within our studied weight range, maximum thermal conductivity (6-fold increase compared to pure wax) is obtained for PW weights of 70 to 80 wt %. For higher PW loading (90 wt %), the thermal conductivity drops to about 3.5 times that of the pure PW due to more wax added into the nanotube sponge. For the 90 wt % wax composite, the nanotube content is 10 wt % and the composite behavior is more like that of pure wax, with similar solid conductivity/liquid conductivity ratios. For the 80 wt % wax composite, the nanotube content increases to 20 wt % and the enhancement of thermal conductivity seems to be saturated.

In addition, our PW–CNTS composites show very stable performance during repeated phase change processes. Figure 2d shows the DSC curves of a 90.5 wt % composite tested for 100 cycles under the same conditions, in which the portions corresponding to wax melting and freezing have a very small shift for all the cycles. Such high reversibility was also observed for composites with other PW loadings of 76–91 wt % (each tested for 11 cycles) (Figure S7). This property is important for recycled use of phase change materials without degradation in heat storage capacity. In the DSC curves, the low-temperature features (<5 °C) are related to the solid phase transition of wax and are less important here because energy storage belongs to the high-temperature region, where wax melting occurs.

The increase of phase change enthalpy and thermal conductivity should be attributed to the intermolecular interaction between carbon nanotubes and paraffin. Recent research has demonstrated that the addition of nanotubes can greatly improve the enthalpy of PCMs, in which intermolecular attraction based on the Lennard–Jones potential is the main reason.[20] We executed a high-energy X-ray diffraction experiment to investigate a related mechanism (see Methods

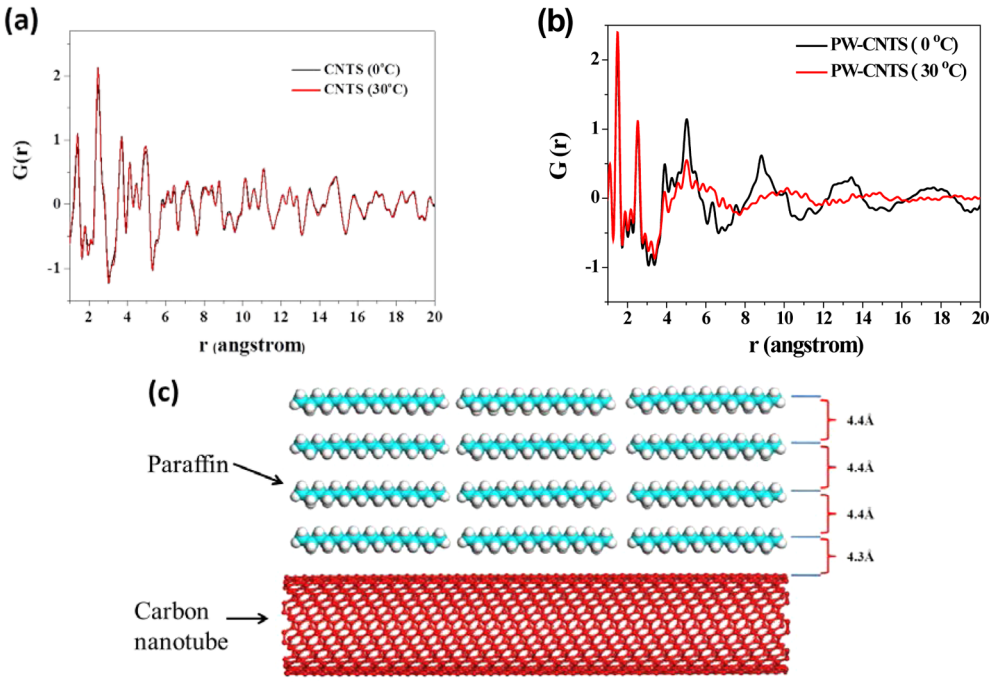

Figure 3. High-energy X-ray diffraction characterization on PW−CNTS composites. (a) Pair distribution function (PDF) curves of an empty sponge (without PW infiltration) at temperatures of 0 and 30 °C, respectively. (b) PDF curves of a PW−CNTS composite at 0 and 30 °C, respectively, showing the broadening of four main peaks at *r* = 4.3, 8.7, 13.1, and 17.5 Å when PW changes from the solid (0 °C) to liquid (30 °C) state. (c) Illustration of the PW molecules with a layer distance of 4.4 Å (top blue) and an interfacial distance of 4.3 Å to a nanotube in contact (bottom red).

for details) and obtained pair distribution function (PDF) data to analyze the interaction type and intermolecular distance for both an empty CNTS and a 96 wt % composite at 0 °C (solid state) and 30 °C (liquid), respectively. As shown in Figure 3a, the patterns of pure CNTS have no change with increasing temperature. In the PW−CNTS composite, the C−C bonds of nanotubes and paraffin remain intact in the low *r* range of 1−4 Å at both 0 and 30 °C; however, the peaks corresponding to the interaction distance and type in the upper *r* range (4−20 Å) are broadened out or even disappear (Figure 3b). In this regard, we propose that four main peaks located at 4.3, 8.7, 13.1, and 17.5 Å of the composite at 0 °C in Figure 3b indicate representative distances between the C atoms of nanotubes and those of paraffin, respectively, with a layer separation of 4.4 Å in paraffin molecules (Figure 3c). A decreased C−C separation (4.3 Å) at the immediate nanotube−paraffin interface suggests the presence of remarkable intermolecular C−H···π interactions.[23−25] In our composite, there are plenty of C−H bonds in paraffin and delocalized π electrons on the surface of nanotubes. Consequently, extensive C−H···π interactions formed at the PW−nanotube interfaces would affect the phase change enthalpy of paraffin. On the other hand, the compressive stress applied by the nanotubes on the melting PW during its volume expansion also could inhibit the solid-to-liquid transition, resulting in increased system enthalpy (Figure 3c). Through such interactions, it is possible to tailor the phase change temperature and increase the enthalpy of PCMs.

Energy storage of our PW−CNTS composites can be realized by electroheat or photothermal routes. Because of the highly conductive embedded nanotube network, we can directly apply an electric potential on the bulk composite to trigger electroheat storage. Current−voltage (*I*−*V*) tests show that the current flowing through a piece of empty CNTS under a constant bias of 1.4 V is stabilized at about 82 mA, giving a very low resistance of 17 Ω. The resistance of a composite with 87 wt % PW content remains small (25 Ω) for both solid and liquid states, indicating that the PW infiltration and subsequent melting do not disturb the original nanotube percolation (Figure 4a). This property is distinct from previous PCMs with dispersed nanomaterials whose percolation network cannot be maintained during phase change. For an empty CNTS placed in an environmental temperature of 15 °C, applying a constant voltage of 1.40 to 1.75 V causes the sample temperature to rise abruptly during the initial 200 s and reach an equilibrium state where heat dissipation from the heated CNTS to the environment balances the energy input (Figure 4b). Correspondingly, a larger input voltage results in a higher equilibrium temperature. Upon removal of the applied voltage, the sample temperature drops immediately to close to that of the environment.

When we apply a similar voltage on a PW−CNTS composite, the temperature increase is slowed compared

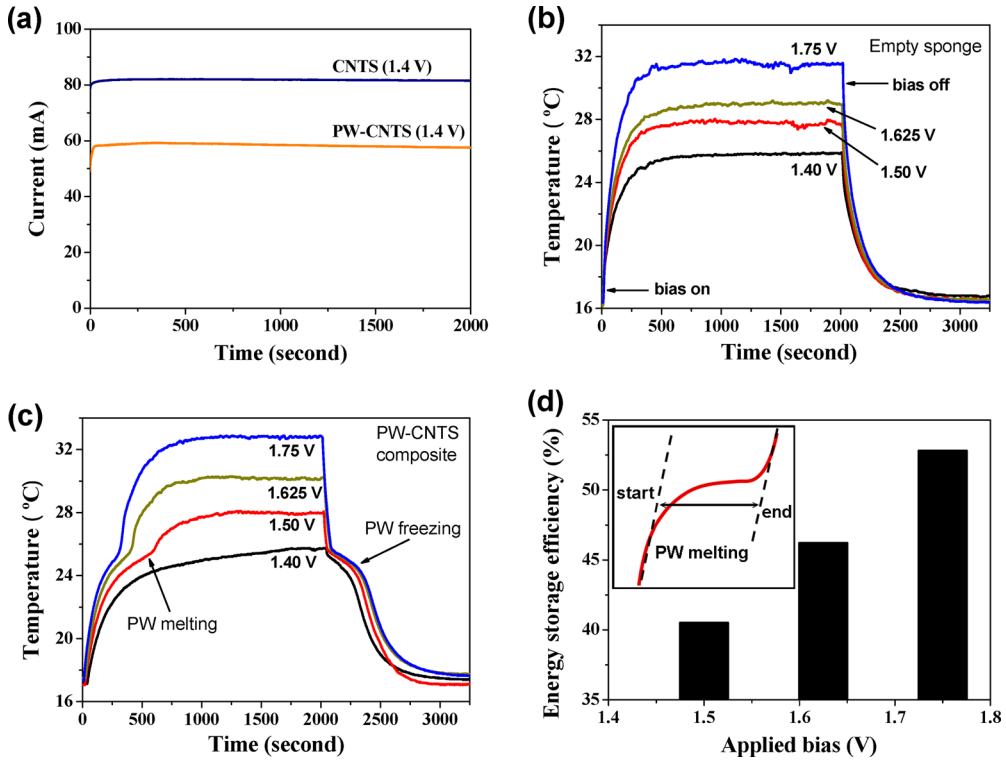

Figure 4. Thermal energy storage by electroheat conversion. (a) Plots of recorded electrical current passing through an empty CNTS and a PW-infiltrated CNTS composite under a constant bias of 1.4 V for an elapsed time of 2000 s. (b) Temperature evolution of an empty sponge under applied voltages of 1.40, 1.50, 1.625, and 1.75 V, respectively. Each bias was maintained for about 2000 s and then removed. (c) Temperature evolution of a PW–CNTS composite under the same bias conditions. Melting of PW occurs during the temperature rise (arrow points to the inflection point where melting finishes), and freezing can be seen after the removal of applied bias (arrow points to the convex region where temperature drops much slower than that seen for an empty sponge). (d) Calculated electroheat energy storage efficiencies for the PW–CNTS composite driven by different voltages (inset shows the tangential method for determining the starting and terminating points of phase change).

to the empty CNTS because of the addition of PW (Figure 4b). For input voltages in the range 1.5 to 1.75 V, the slopes of the temperature–time plots gradually decrease until an inflection point, after which the temperature starts to increase fast again, indicating that PW melting starts and terminates in the region approaching the minimum slope (Figure 4c). The inflection points under voltages of 1.5 to 1.75 V occur at temperatures of 25 to 26 °C, consistent with the phase change temperature of the same loading composite (peak position at 27 °C), as shown in Figure 2a. After phase change finishes, the composite temperature increases rapidly until the equilibrium state. At a lower voltage of 1.4 V, there is no inflection point in the temperature curve, indicating that PW in the composite has not all melted during the period (2000 s) and a critical voltage for complete phase change is about 1.5 V. After terminating the applied voltages, all temperature curves immediately drop to the freezing point of wax (about 25 °C, see Figure 4c), and the appearance of another inflection point in each curve is associated with subsequent PW freezing during cooling.

The above results indicate that electrical potential can enable the phase change of PW–CNTS composites, and the stored heat energy can be released during the cooling process. The electroheat storage is enabled by efficient heat transfer from the conductive nanotube networks to the surrounding PW throughout the composite. When a current passes through the composite, Joule heat is generated by the resistance of individual nanotubes and also the contact resistance in the network, and the main heat transfer mechanism involves solid-to-solid heat conduction at the PW–nanotube interface. We have calculated the electroheat storage efficiency (η) by the ratio of stored heat in PW, which is the total mass of PW enclosed in the composite (m) times its enthalpy (ΔH), with respect to the received electrical energy during the phase change period, which is the product of voltage (U), current (I), and time (t). Therefore the energy storage efficiency in our system is defined as $\eta = (m\Delta H)/UIt$ assuming that all encapsulated PW material has participated in the phase change. The starting and terminating points of the phase change are determined by the tangential method to obtain the value of t (inset of Figure 4d, data summarized in Table S1). Thus the electro-to-heat storage efficiency is about 40.6% under 1.5 V and 52.5% under higher voltage (1.75 V) (Figure 4d). The phase change period is shortened under higher voltage; therefore convection heat loss from the heated

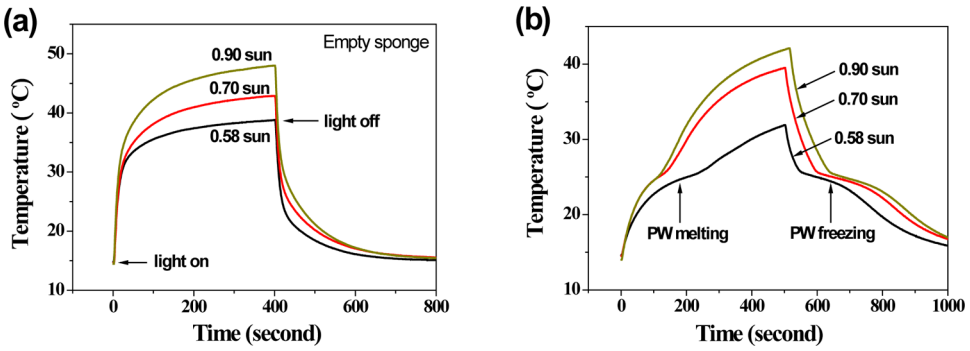

Figure 5. Thermal energy storage by simulated sunlight absorption. (a) Temperature evolution curves of an empty sponge illuminated by simulated sunlight (AM 1.5) at intensities of 58, 70, and 90 mW/cm^2, showing abrupt increase and decrease of temperature when light turns on and off. (b) Temperature evolution curves of a PW–CNTS composite under the same illumination conditions, showing that PW melting and freezing occur during the heating and cooling processes.

composite (exposed to air) to the environment is reduced, resulting in enhanced efficiency. The energy storage efficiency could be further improved by an appropriate thermal sealing technique to prevent or minimize heat dissipation to the environment.

Not only can electrical energy be stored as heat in our composites, light energy also can be utilized. Vertically aligned nanotube arrays behave as a blackbody due to effective light scattering and trapping.[26] Our CNTS is highly porous and appears black in the original state, indicating high absorption of sunlight. The presence of nanotubes enhances photon absorption and in turn can heat the PW in the composite. Under simulated solar illumination (AM 1.5) at controlled intensities of 58, 70, and 90 mW/cm^2, respectively, the surface temperature of a blank CNTS increases abruptly from 15 °C to more than 30 °C and then gradually reaches equilibrium over a period of 400 s (Figure 5a). When the incident light turns off, the temperature drops quickly in a manner similar to the removal of voltage as shown in Figure 4b. When a PW–CNTS composite (87 wt % loading) is exposed to light, phase change occurs at temperatures close to 25 °C under all light intensities, as seen from the reduced slope and inflection point in each curve (Figure 5b). Correspondingly, we see heat releasing from the composite during the freezing of PW after turning off the light. Similarly, the photothermal storage efficiency can be estimated by the ratio of stored energy in PW (mass times enthalpy) with respect to the light energy received by the sample area (1.8 × 3.5 cm^2) over the phase change period (determined by the tangential method as in Figure 4d). Therefore, our composites have energy storage efficiencies of 40% to 60% (Table S2), which increase with higher light intensity. We have not found many reports on the energy storage efficiency of similar composites, especially on the electro-to-heat conversion. A recent study on a dye-grafted phase change material shows a sunlight-to-heat storage efficiency of more than 90% by simulating light irradiation at a wavelength (half-wave width of 80 nm) corresponding to maximum dye absorption using an optical filter.[27] In comparison, our efficiencies are relatively lower and calculated based on the entire solar spectrum (at air mass 1.5 and calibrated light intensities).

CONCLUSIONS

In conclusion, we report a carbon nanotube sponge-encapsulated paraffin wax composite that can store thermal energy by applying a small voltage or light absorption. The phase change enthalpy and thermal conductivity of the composite can be tailored by the respective fractions of wax and nanotubes. Compared to previous phase change materials dispersed with carbon nanotubes or graphene sheets, our composite maintains a highly conductive nanotube network during paraffin melting and freezing, and the voltage for enabling phase change could even be supplied by a portable lithium-ion battery. Our electro- and photodriven phase change composites have wide applications in areas related to energy conversion and storage.

METHODS

Synthesis of CNTS and PW–CNTS Composites. Macroscopic, freestanding carbon nanotube sponges were synthesized by chemical vapor deposition using ferrocene and 1,2-dichlorobenzene as the precursors, as reported in our previous work.[16] The sponge samples collected from the inside wall of the reaction quartz tube were cut into rectangular blocks for making composites. We employed a solution-assisted infiltration process to make phase change composites. Refined paraffin wax (oil impurity <0.8%) was perchased from Sinopec Nanyang Wax Refining Factory, Henan Province, China. A certain amount of wax was dissolved in CH_2Cl_2 to make a solution at 0.03 g·mL^{-1} concentration, and the solution was dripped onto the surface of a given weight CNTS. Transferred paraffin solution was completely sucked into the porous CNTS quickly, and the infiltrated solution volume was controlled to make composites with different paraffin loadings. After that, the sample was placed in a loft drier under low pressure to let the CH_2Cl_2 solvent

evaporate and formed a densified solid PW−CNTS composite with large volume shrinkage. The loading percentage of wax was calculated based on the weight difference before and after infiltration (after solvent evaporation under vacuum) relative to the original sponge weight.

Thermal Conductivity Measurements. These were carried out with a hot-wire thermal conductivity instrument (Xiatech TC3010), and a circulating oil bath was used to adjust the temperature. To test the thermal conductivity, we put the hot wire between two same sponge samples and placed a weight on top of the stacked samples. The sponge can make good contact with the hot wire under slight compression due to its mechanical flexibility. For each sample, we performed five measurements and obtained an average value as its conductivity.

Characterization of Electrical to Thermal Energy Storage. A thermal resistance (Pt100) was inserted into the target material (a CNTS or a PW−CNTS composite) to measure the temperature inside the sample *in situ* during the heating and cooling processes. The accuracy of the Pt100 thermal resistance is ±0.15 °C. The sponge or composite was connected to an electrochemical workstation (Zahner ennium/IM6) with two copper wires as electrodes. Each copper wire was plugged into the composite near the side surface to make good electrical contact with the nanotube network in a two-probe configuration. The samples were covered by a plastic box to minimize the environmental influence of air convection. A certain bias (1.4 to 1.75 V) was applied to the sample by the workstation for about 2000 s and then stopped, while the current flowing through the sample was recorded simultaneously. Temperature evolution of the sample was recorded by a data aquisition system (ICDAM-7033 and ICDAM-7520) connected to the thermal resistance.

Characterization of Photothermal Energy Storage. Samples of CNTS or PW−CNTS composites were illuminated by simulated sunlight using a solar simulator (Newport Thermo Oriel 91195A-1000) at controlled intensities (58−90 mW/cm^2). The sample temperature was measured by a Pt100 thermal resistance and recorded by a data aquisition system using the same configuration. The samples were placed in a transparent and sealed plastic box. The light intensity was calibrated by a standard Si solar cell (91150 V). Each sample was exposed to light for 400 to 500 s; after that, theh light was turned off to let the sample cool.

High-Energy X-ray Diffraction. The high-energy X-ray diffraction experiment was excuted to investigate the intermolecular interaction mechanism at the 11-ID-C beamline at the Advanced Photon Source at Argonne National Laboratory, with an energy fixed at 115 keV and a wavelength at 0.10804 Å. An Oxford Cryosystems Cryostream setup (80−400 K) was employed to control the temperature of all the samples measured, which were loaded into kapton capillaries with a diameter of 1.0 mm. The pair distribution function data were obtained by a Fourier transformation by using the PDFgetX2 software package. $F(Q)$ was truncated at Q_{max} = 20 Å^{-1} to avoid the unfavorable signal-to-noise ratio at the high-Q region.

Measurements on the Nanotube Sponge Surface Area. A sample tube of a known weight was loaded with 30 mg of sample and sealed using a TranSeal. Samples were degassed at 120 °C for 3 h on a QUANTACHROME Autosorb-iQ analyzer until the outgas rate was no more than 1 mTorr/min. The degassed sample and sample tube were weighed precisely and then transferred back to the analyzer (with the TranSeal preventing exposure of the sample to the air after degassing). The outgas rate was again confirmed to be less than 1 mTorr/min. Adsorption isotherms were measured at 77 K in a liquid nitrogen bath.

SEM, DSC, and TGA Measurements. SEM characterization was performed using a field-emission microscope (Hitachi-s4800) operated at 10 kV. DSC data were obtained with a differential scanning calorimeter (Setaram DSC 131 evo) with an Al 30 μL pan. All the sample weights are between 1 and 5 mg, and the temperature change rate is 5 °C/min under protection of Ar. The TGA curves were obtained with a thermogravimetric analysis instrument (TA SDT-Q600), and all sample weights were between 1 and 3 mg.

Conflict of Interest: The authors declare no competing financial interest.

Acknowledgment. This work was supported by National Basic Research Program of China No. 2009CB939902 and Beijing Natural Science Foundation (Program No. 8112017). The authors acknowledge Dr. Yang Ren at APS, 11-ID-C for the high-energy X-ray diffraction experiment (proposal number GUP-25238), and the lab of Prof. Kunlin Wang and Dehai Wu from Tsinghua University for help in synthesizing carbon nanotube sponges.

Supporting Information Available: This material is available free of charge *via* the Internet at http://pubs.acs.org.

REFERENCES AND NOTES

1. Kenisarin, M.; Mahkamov, K. Solar Energy Storage Using Phase Change Materials. *Renewable Sustainable Energy Rev.* **2007**, *11*, 1913–1965.
2. Nomura, T.; Okinaka, N.; Akiyama, T. Waste Heat Transportation System, Using Phase Change Material (PCM) from Steelworks to Chemical Plant. *Resour. Conserv. Recycl.* **2010**, *54*, 1000–1006.
3. Nomura, T.; Oya, T.; Okinaka, N.; Akiyama, T. Feasibility of an Advanced Waste Heat Transportation System Using High-Temperature Phase Change Material (PCM). *Isij. Int.* **2010**, *50*, 1326–1332.
4. Huang, M. J.; Eames, P. C.; McCormack, S.; Griffiths, P.; Hewitt, N. J. Microencapsulated Phase Change Slurries for Thermal Energy Storage in a Residential Solar Energy System. *Renewable Energy* **2011**, *36*, 2932–2939.
5. Farid, M. M.; Khudhair, A. M.; Razack, S. A. K.; Al-Hallaj, S. A Review on Phase Change Energy Storage: Materials and Applications. *Energy Convers. Manage.* **2004**, *45*, 1597–1615.
6. Khudhair, A. M.; Farid, M. M. A Review on Energy Conservation in Building Applications with Thermal Storage by Latent Heat Using Phase Change Materials. *Energy Convers. Manage.* **2004**, *45*, 263–275.
7. Sharma, A.; Tyagi, V. V.; Chen, C. R.; Buddhi, D. Review on Thermal Energy Storage with Phase Change Materials and Applications. *Renewable Sust.ainable Energy Rev.* **2009**, *13*, 318–345.
8. Karaipekli, A.; Sarinodot, A.; Bicer, A. Synthesis, Characterization, Thermal Properties of a Series of Stearic Acid Esters as Novel Solid-Liquid Phase Change Materials. *Mater. Lett.* **2009**, *63*, 1213–1216.
9. Sumin, K.; Drzal, L. T. High Latent Heat Storage and High Thermal Conductive Phase Change Materials Using Exfoliated Graphite Nanoplatelets. *Sol. Energy Mater. Sol. Cells* **2009**, *93*, 136–142.
10. Inaba, H.; Tu, P. Evaluation of Thermophysical Characteristics on Shape-Stabilized Paraffin as a Solid-Liquid Phase Change Material. *Heat Mass Transfer* **1997**, *32*, 307–312.
11. Wang, J.; Xie, H.; Xin, Z. Thermal Properties of Paraffin Based Composites Containing Multi-Walled Carbon Nanotubes. *Thermochim. Acta* **2009**, *488*, 39–42.
12. Yavari, F.; Fard, H. R.; Pashayi, K.; Rafiee, M. A.; Zamiri, A.; Yu, Z.; Ozisik, R.; Borcatasciuc, T.; Koratkar, N. Enhanced Thermal Conductivity in a Nanostructured Phase Change Composite Due to Low Concentration Graphene Additives. *J. Phys. Chem. C* **2011**, *115*, 8753.
13. Wang, J.; Xie, H.; Xin, Z.; Li, Y.; Yin, C. Investigation on Thermal Properties of Heat Storage Composites Containing Carbon Fibers. *J. Appl. Phys.* **2011**, *110*, 094302.
14. Phadungphatthanakoon, S.; Poompradub, S.; Wanichwecharungruang, S. P. Increasing the Thermal Storage Capacity of a Phase Change Material by Encapsulation: Preparation and Application in Natural Rubber. *ACS Appl. Mater. Interfaces* **2011**, *3*, 3691–3696.
15. Zheng, R.; Gao, J.; Wang, J.; Chen, G. Reversible Temperature Regulation of Electrical and Thermal Conductivity Using Liquid−Solid Phase Transitions. *Nat. Commun.* **2011**, *2*, 289–295.
16. Gui, X.; Wei, J.; Wang, K.; Cao, A.; Zhu, H.; Jia, Y.; Shu, Q.; Wu, D. Carbon Nanotube Sponges. *Adv. Mater.* **2010**, *22*, 617–621.
17. Gui, X.; Cao, A.; Wei, J.; Li, H.; Jia, Y.; Li, Z.; Fan, L.; Wang, K.; Zhu, H.; Wu, D. Soft, Highly Conductive Nanotube Sponges

and Composites with Controlled Compressibility. *ACS Nano* **2010**, *4*, 2320–2326.
18. Zeng, J. L.; Cao, Z.; Yang, D. W.; Xu, F.; Sun, L. X.; Zhang, X. F.; Zhang, L. Effects of MWNTS on Phase Change Enthalpy and Thermal Conductivity of a Solid-Liquid Organic PCM. *J. Therm. Anal. Calorim.* **2009**, *95*, 507–512.
19. Bayramoglu, E. C. Thermal Properties and Stability of N-Octadecane Based Composites Containing Multiwalled Carbon Nanotubes. *Polym. Compos.* **2011**, 904–909.
20. Shaikh, S.; Lafdi, K.; Hallinan, K. Carbon Nanoadditives to Enhance Latent Energy Storage of Phase Change Materials. *J. Appl. Phys.* **2008**, *103*, 094302.
21. Balandin, A. A. Thermal Properties of Graphene and Nanostructured Carbon Materials. *Nat. Mater.* **2011**, *10*, 569–581.
22. Assael, M. J.; Antoniadis, K. D.; Wakeham, W. A. Historical Evolution of the Transient Hot-Wire Technique. *Int. J. Thermophys.* **2010**, *31*, 1051–1072.
23. Kim, K. S.; Tarakeshwar, P.; Lee, J. Y. Molecular Clusters of Pi-Systems: Theoretical Studies of Structures, Spectra, and Origin of Interaction Energies. *Chem. Rev.* **2000**, *100*, 4145–4185.
24. Tarakeshwar, P.; Choi, H. S.; Kim, K. S. Olefinic vs Aromatic Pi-H Interaction: A Theoretical Investigation of the Nature of Interaction of First-Row Hydrides with Ethene and Benzene. *J. Am. Chem. Soc.* **2001**, *123*, 3323–3331.
25. Tsuzuki, S.; Honda, K.; Uchimaru, T.; Mikami, M.; Tanabe, K. Origin of the Attraction and Directionality of the Nh/Pi Interaction: Comparison with OH/Pi and CH/Pi Interactions. *J. Am. Chem. Soc.* **2000**, *122*, 11450–11458.
26. Hsieh, K. C.; Tsai, T. Y.; Wan, D.; Chen, H. L.; Tai, N. H. Iridescence of Patterned Carbon Nanotube Forests on Flexible Substrates: From Darkest Materials to Colorful Films. *ACS Nano* **2010**, *4*, 1327–1336.
27. Wang, Y.; Tang, B.; Zhang, S. Novel Organic Solar Thermal Energy Storage Materials: Efficient Visible Light-Driven Reversible Solid-Liquid Phase Transition. *J. Mater. Chem.* **2012**, *22*, 18145–18150.